Journal of
Materials Chemistry C

RSC Publishing

HIGHLIGHT

View Article Online
View Journal | View Issue

Cite this: *J. Mater. Chem. C*, 2013, **1**, 4190

Harnessing self-assembly strategies for the rational design of conjugated polymer based materials

Rachel C. Evans*[ab]

Received 22nd March 2013
Accepted 23rd April 2013

DOI: 10.1039/c3tc30543k

www.rsc.org/MaterialsC

Targeted control of the aggregation, morphology and optoelectronic properties of conjugated polymers is critical for the development of high performance optoelectronic devices. In this Highlight, recent advances in the use of self-assembly approaches to strategically manipulate the order, conformation and spatial distribution of conjugated polymers in various states (*e.g.* solution, gels, films, solids) are discussed. Emphasis is placed on the complex relationship that exists between molecular composition, self-assembly and supramolecular organisation and their consequential influence on the optoelectronic properties and device performance.

1 Introduction

Conjugated polymers (CP) are now well-established as the basis for flexible organic electronic devices such as light-emitting diodes, field-effect transistors, optical sensors and solar cells.[1–4] Device performance has been shown to critically depend on the optoelectronic properties and nanoscale morphology of the conjugated polymer, which are intrinsically linked.[5,6] Solution-phase processing methods such as inkjet or screen printing provide a route to facile, low cost fabrication of these devices.[7] However, the nanostructure of conjugated polymer films deposited using such methods will be influenced by the conformation of the polymer species present in solution. Similarly, the semiconductor-like optical and electronic properties of conjugated polymers also depend explicitly on the physical conformation of the polymer chains. The ability to control the polymer morphology and its interdependent optoelectronic properties is thus an important step towards the rational optimisation of organic electronic devices.

A variety of strategies have been investigated to exert control over polymer conformation and to reduce chain aggregation. These include using polymer blends,[8,9] preparing self-assembled Langmuir–Blodgett films,[10] or by confining the CP within the channels of porous templates.[11–13] The addition of long aliphatic side-chains,[14] bulky pendant substituents[15] or dendritic side groups[16] also help to diminish interchain aggregation. Cutting-edge techniques such as nanoimprint lithography have also been used to fabricate large-area ordered CP nanostructures.[17]

In recent years, self-assembly approaches have increasingly emerged as an elegant bottom-up approach for the design and fabrication of reproducible nanoscale structures both in solution and the solid state.[18–24] Self-assembly involves the spontaneous association of organic, inorganic or hybrid building blocks, mediated by non-covalent interactions (*e.g.* electrostatic, van der Waals and hydrophobic forces, π–π stacking, hydrogen bonding), into stable, well-defined aggregates that exhibit structural and morphological organisation across multiple length scales.[25] While these non-covalent interactions may be relatively insignificant in isolation, when operating in unison they act as a powerful driving force for cooperative assembly over multiple building blocks. Self-assembly offers unprecedented potential as a route for obtaining simultaneous control over the aggregation and optoelectronic properties of

[a]*School of Chemistry, University of Dublin Trinity College, College Green, Dublin 2, Ireland. E-mail: raevans@tcd.ie*
[b]*Centre for Research on Adaptive Nanostructures and Nanodevices (CRANN), Trinity College Dublin, Dublin 2, Ireland*

Rachel C. Evans is currently the Ussher Assistant Professor in Device Fabrication in the School of Chemistry, Trinity College Dublin. She obtained her MChem (2002) and PhD (2007) from Swansea University, having spent time at the University of Aveiro as a Marie Curie Training fellow. She was subsequently a Marie Curie postdoctoral fellow at the Université Paris-Sud, before being awarded a research fellowship from the Fundação para a Ciência e a Tecnologia (FCT) to work jointly between the Universities of Coimbra and Aveiro, Portugal (2008–2009). Her research focuses on bridging the interface between materials and device photochemistry, with an emphasis on the design and development of photoactive hybrid materials for application in optical and photovoltaic devices.

conjugated polymers due to their immense structural versatility. Modification of the structure and arrangement of the repeat unit, the molecular weight, the chemical groups that make up the chain ends or side chains, or any combination of the above, enables facile tailoring of both the optoelectronic properties and the tendency towards self-assembly (*e.g.* through the introduction of charged, hydrophilic, hydrophobic segments *etc.*).[26]

In this Highlight, recent examples towards the development of integrated conjugated polymer systems, exhibiting controlled orientation and/or organisation of the polymer chains through virtue of self-assembly are described. We first consider how the nature of the solvent can be exploited to either induce or inhibit interchain interactions in solution, thereby modulating the aggregation state of the polymer. The use of solvent-mediated self-assembly to promote the evolution of more ordered aggregates, such as polymer dots, sheets and vesicles in amphiphilic polymers is then discussed. We then progress to all-organic hybrid conjugated polymer aggregates, whereby co-assembly of the CP with organic building blocks (*e.g.* surfactants) leads to the formation of exotic, self-organised architectures, both in solution and the solid state. Finally we consider organic–inorganic hybrid CP supramolecular assemblies, where weak physical interactions at the phase interface are used to introduce order into either or both phases. In all cases, we focus on the type of non-covalent interaction(s) driving the self-assembly process and attempt to unravel the correlation between the optoelectronic properties and the structural organisation in these materials to their application in organic electronic devices.

2 Solvent-mediated self-assembly

2.1 Aggregation of CPs in solution: photophysical consequences

The physical conformation of a conjugated polymer chain is strongly influenced by the solvent environment. In turn, modifications to the chain conformation (and polymer concentration) can affect how easily independent CP chains can aggregate together in a way that influences the optoelectronic properties.[5] The hydrophobic, structurally rigid backbone means that conjugated polymers often exhibit low solubility, which is due to a combination of a small positive entropy of dissolution (due to reduced conformational mobility in solution) and a small negative enthalpy of dissolution (due to efficient molecular packing in the solid state).[27] Polymer solubility may be improved by covalently linking flexible side chains to the backbone. The addition of hydrophobic side chains renders the polymer soluble in most organic solvents, whereas in contrast, polymers decorated with hydrophilic or ionic side chains are soluble in polar solvents and often even water.[15,28,29] In addition, CPs containing ionic groups on their side chains exhibit the charge-mediated behavior typical of polyelectrolytes, giving rise to the sub-class of materials known as conjugated polyelectrolytes (CPEs).[15,27,28] However, although CPEs may appear to completely dissolve in pure water at the macroscopic level, in practice, they tend to exist as loose aggregates due to a complex interplay between π–π stacking, hydrophobic and various intra- and interchain interactions.[30–34]

Aggregation of individual chains extends the effective conjugation length, which is manifested as a bathochromic (red) shift in the absorption and photoluminescence spectra.[33] Simultaneously, aggregation leads to enhanced exciton mobility and a consequent decrease in the photoluminescence quantum yield, Φ_{PL}, is commonly observed due to the increased probability of electron–hole recombination at non-radiative trap sites.[34] The addition of small quantities of polar co-solvents (*e.g.* acetonitrile, methanol, 1,4-dioxane) to aqueous CPE solutions has been shown to dissociate molecular aggregates, which reverses the above trends in the photophysical properties, *i.e.* yielding blue-shifted absorption and emission maxima and an increase in Φ_{PL}.[30–32] The chemical nature of the side chains therefore plays a pivotal role in defining the solubility and conformation of the polymer in a given medium. It should be noted, however, that aggregation has been shown to increase the emission intensity for some conjugated polymers, rather similar to the Aggregation-Induced Emission (AIE) phenomenon observed in some non-planar conjugated small molecules.[35] AIE active molecules, such as the archetypal hexaphenylsilole (HPS), typically exhibit a propeller-like structure containing rotor and stator functional groups.[36] In dilute solution, intramolecular rotations against the stator (*e.g.* rotation of the 6 phenyl rings against silole in HPS) result in non-radiative annihilation of the excited state, rendering the molecule non-luminescent. However, in the aggregated state, non-radiative deactivation is significantly reduced due to physical restraints on both intramolecular rotations and π–π stacking interactions, which preferentially results in radiative deactivation of the excited state (*i.e.* the photoluminescence is 'switched on').[36] Aggregation-enhanced emission (AEE) has been observed for some poly(1-phenyl-1-alkyne)s[37] and poly(diphenylacetylene)s,[38] which both contain a phenyl rotor(s) and an olefin stator in their repeat units. Steric hindrance partially inhibits intramolecular rotation of the phenyl rings in these polymers, such that they are already emissive in dilute solution. Upon aggregation, however, this effect is amplified, resulting in the observed enhancement of the photoluminescence.

2.2 Conjugated polymer nanoparticles (polymer dots)

Spherical CP nanoparticles (polymer dots) can be obtained by exploiting changes in the polymer solubility and therefore conformation in different polarity media.[39–43] Rapid injection of a miscible organic solution of a neutral conjugated polymer into an excess of water (the *reprecipitation method* – see Fig. 1) results in the self-assembly of neutral conjugated polymers into discrete nanoparticles, promoted by the driving force for aggregation exerted by the hydrophobic backbone on introduction into the aqueous environment. Nanoparticle formation is typically confirmed by the observation of a red-shift in the absorption and photoluminescence spectra compared to the parent CP solution, in conjunction with light scattering and electron microscopy studies.[39–43]

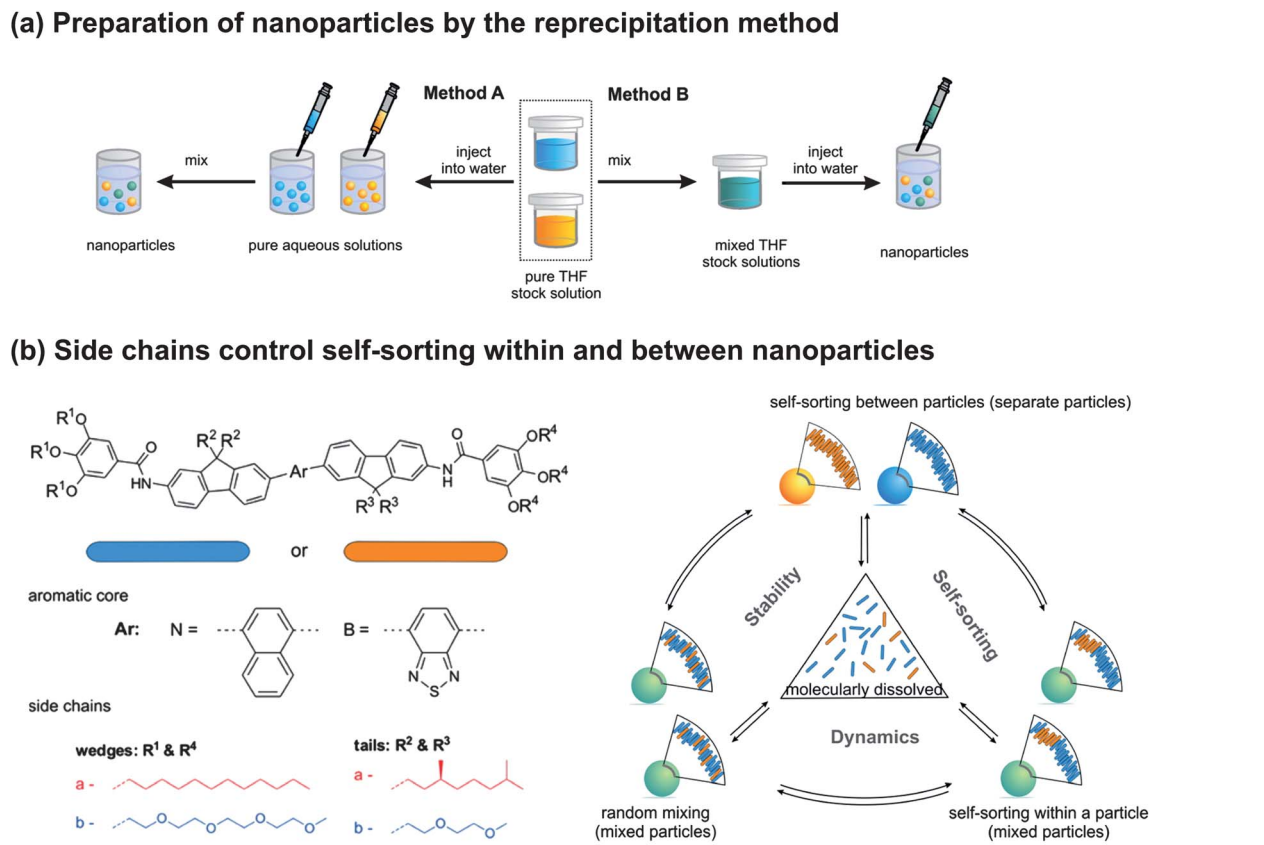

Fig. 1 (a) Preparation of CP nanoparticles using the reprecipitation method. (b) Structures of the fluorene co-oligomers and the resulting self-assembled states of bi-component nanoparticles containing naphthalene (blue) and benzothiadiazole (orange) motifs. Adapted with permission from ref. 42. Copyright 2013 American Chemical Society.

Schenning and co-workers recently demonstrated that polarity of the side chains also influences the size, stability and fluorescence quantum yield of nanoparticles prepared from non-ionic fluorene co-oligomers using this approach.[42] Nanoparticles derived from π-conjugated fluorene co-oligomers containing non-polar side chains were more stable, smaller and generally had a higher Φ_{PL} than nanoparticles prepared from hydrophilic analogues (Fig. 1). Energy transfer dynamics between donor (naphthalene) and acceptor (benzothiadiazole) chromophores incorporated in the co-oligomer backbone revealed that no oligomer exchange occurred between preformed nanoparticles for the hydrophobic oligomers, whereas in contrast, molecular exchange took place both at room temperature or after annealing in the case of hydrophilic oligomers. Moreover, it was observed that nanoparticles prepared from solutions containing a mixture of naphthalene- and benzothiadiazole-fluorene co-oligomers exhibited self-sorting, resulting in either the formation of distinct domains within the particles or the formation of separate nanoparticles, due to the differing solubility gradients induced by the polarity of the side-chains. These results indicate that by appropriate design of the polarity of the polymer side chains it should be possible to prepare multicomponent nanostructures with selective macroscopic properties capable of mimicking the media they are in, which would be highly advantageous for sensing and imaging applications.

2.3 Amphiphilic CPs: blackberries, rods and vesicles

Conjugated polyelectrolytes are inherently amphiphilic: the addition of ionic side chains to the hydrophobic polymer backbone introduces a distinct solubility gradient across the polymer. For synthetic simplicity, the terminal ionic groups are typically small anions (*e.g.* SO_3^{2-}, PO_3^{2-}) or cations (*e.g.* NR_3^+); however, there is no restriction on the size or charge of the moiety which may be introduced. For example, a series of poly(phenylene ethynylene) (PPE) conjugated polymers containing side-chains terminating with a hexamolybdate anionic cluster $[Mo_6O_{19}]^{2-}$, approximately 1 nm in size, has been demonstrated.[44,45] Large polyoxometalate (POM) macro-anions are known to self-assemble into vesicle-like single-layered blackberry structures in polar solvents, driven by counterion-mediated attraction and hydrogen bonding.[46,47] Peng, Liu and co-workers recently demonstrated that hybrid PPE–POM polymers mimic the solution self-assembly behaviour of the parent macro-anions:[45] in non-polar solvents such as toluene, the polymers exhibit amphiphilicity and self-assemble into reverse vesicle, whereas in polar solvents, the side chains are charged and the polymers assemble into 1D hollow tubular structures typical of polyelectrolytes. POM-containing hybrid polymers have been shown to be good candidates for photovoltaic cells and photocatalytic materials and obtaining such hierarchical organisation of the CP and POM components within a single

nanostructure should significantly enhance their performance.[48]

Differences in the solubility and/or crystallinity of the polymer structure may also be exploited to yield more exotic self-assembled structures. Block copolymers contain two or more immiscible homopolymers that are covalently linked, which naturally exhibit self-assembled nanodomains due to the inherent incompatibility between the blocks.[49–51] The shape and size of these nanodomains are determined by the block ratio, molecular weight, and block–block interaction parameter.[49] Scherf and co-workers have recently reported an elegant synthetic approach to amphiphilic all-conjugated polyelectrolyte block copolymers, in which the blocks exhibit not only different chemical structures, but also differing polarities.[53] Examples include the combination of a hydrophobic, blue-emitting polyfluorene (PF) block such as poly[9,9-bis(2-ethylhexyl)-fluorene] (PF2/6) or poly[9,9-bis(octyl)-fluorene] (PFO) connected to a polar, red-emitting polythiophene (PT) block such as poly[3-(6-trimethylammoniumhexyl)thiophene] (P3TMAHT), poly[3-(6-diethylphosphonatohexyl)thiophene] (P3PHT) or poly[3-(6-pyridylhexyl)thiophene] (P3PyHT) (Fig. 2).[52] The hydrophilic nature of the polythiophene blocks leads to solvent-induced self-assembly in mixtures of selective and non-selective solvents, as observed for PF2/6-P3PHT in water–tetrahydrofuran (THF) or water–hexane[53] or PF2/6-*b*-P3TMAHT in water–THF[54] or water–MeOH.[55] Notably, the self-assembled structures generated in solution are transferred to the solid-state, such that PF2/6-*b*-P3TMAHT forms vesicular nanostructures in drop-cast films prepared from low concentration methanolic solutions (0.03 mg mL^{-1}) (Fig. 2b). Films prepared from solutions at higher concentrations (~5 mg mL^{-1}) lead to a denser coverage of the substrate and a transformation to solid state-like films.[52] Atomic force microscopy (AFM) measurements reveal a transition from vesicular (region 1, Fig. 2a) to a lamellar morphology (region 3, Fig. 2a) with a layer height of *ca.* 35–45 nm, which corresponds to the double lateral dimension of the copolymer bilayers formed following collapse of the vesicles.

The PF2/6 emission spectrum and the P3TMAHT absorption spectrum exhibit significant spectral overlap, such that Förster resonance energy transfer (FRET) from the donor PF2/6 to the acceptor P3TMAHT may be exploited to provide insight into the conformation of the polymer in different media.[54] Since the FRET efficiency depends critically on the donor–acceptor distance, structural reorganisation of PF2/6-*b*-P3TMAHT aggregates in different solvent mixtures will be indicated by a change in the photoluminescence spectrum of the aggregate (Fig. 2b). For example, THF is a non-selective solvent for both the PF2/6 and P3TMAHT blocks. Each block exhibits its characteristic individual photoluminescence (PL) characteristics and no energy transfer is observed, indicating that the majority of PF2/6 and P3TMAHT blocks are outside of the Förster transfer radius, and that the polymer forms aggregates with segregated PF2/6- and P3TMAHT-rich domains. In THF–water

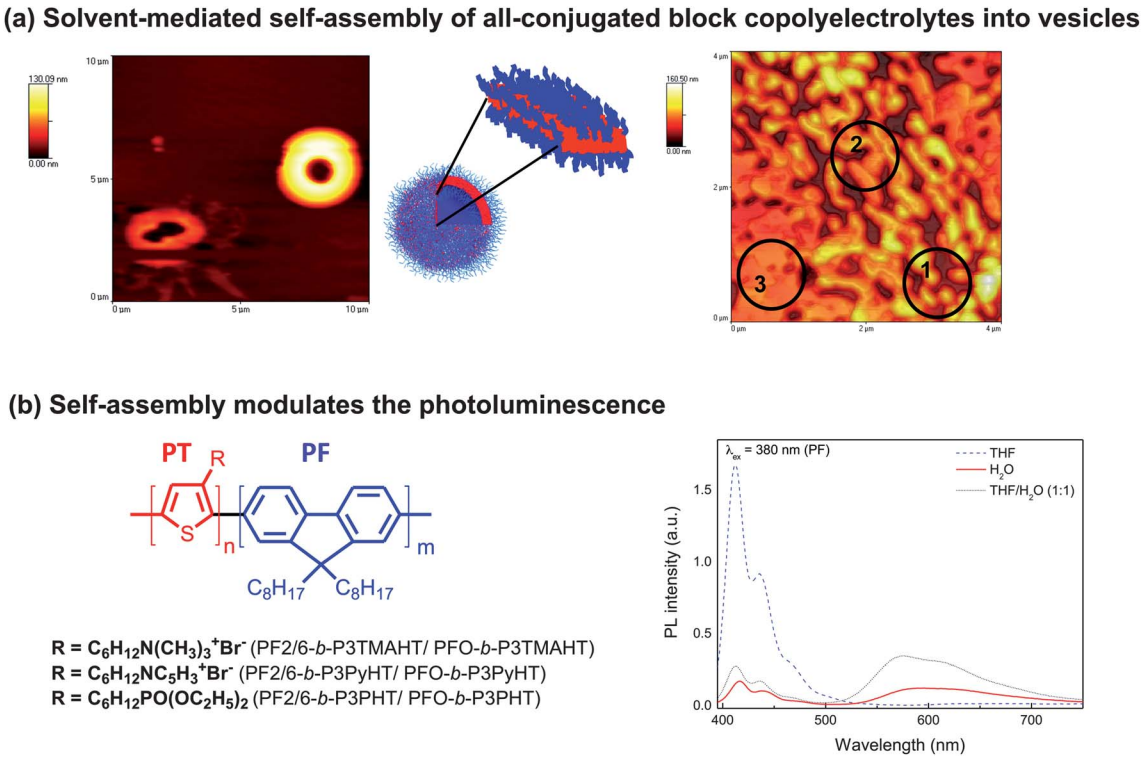

Fig. 2 (a) Left: contact mode AFM image of PF2/6-*b*-P3TMAHT vesicles deposited from MeOH onto a mica substrate (0.3 mg mL^{-1}). Middle: graphical illustration of the vesicle structure. Right: tapping mode AFM images of PF2/6-*b*-P3PyHT deposited from methanolic solution (5 mg mL^{-1}) onto a silica substrate (topography image). (b) Left: structure of all-conjugated PF-PT block copolyelectrolytes. Right: PL spectra of PF2/6-*b*-P3TMAHT in THF (dashed line), water (solid line) and THF–water (1 : 1) (dotted line) on selective excitation of the PF block (λ_{ex} = 380 nm). Adapted from ref. 52.

(1 : 1) selective excitation of the PF2/6 block results in energy transfer, suggesting a closer proximity of distinct blocks. In pure water, poor solubility of the hydrophobic PF2/6 blocks promotes the formation of aggregates in which the PF2/6 blocks are located in the interior, thus minimising polymer–solvent contacts. Small-angle X-ray and neutron scattering (SAXS/SANS) experiments confirmed that PF2/6-*b*-P3TMAHT undergoes a series of structural transitions in solution, with variations in the solubility gradient promoting a transition from aggregates with surface fractal interface (THF), to those with a significant planar component due to the presence of the 2-dimensionally merged ribbon-like aggregates or the fused walls of the observed vesicular nanostructures (THF–water (1 : 1)). Reorganisation of the self-assembly structure is therefore concomitant with distinct solvatochromic changes in the photoluminescence behaviour.

3 All-organic hybrid CPE materials

3.1 CPE–surfactant complexes

The addition of ionic or neutral surfactants at concentrations below the critical micelle concentration (CMC) to aqueous CPE solutions has been shown to break up and disperse polymer aggregates, similarly modifying the photophysical properties as described above for co-solvent addition.[56–59] Recent efforts have focused on understanding the mechanism(s) behind CPE–surfactant association and the subsequent photophysical consequences across several concentration regimes. While size and charge density are critical factors in driving the electrostatic association between the hydrophilic head group and the ionic side chains,[59,60] the role of secondary interactions (*e.g.* hydrophobic, van der Waals, hydrogen bonding, hydration) will undoubtedly determine the shape, size and compactness of the co-assembly structures formed. In a study of the interaction between the anionic sodium poly[2-(3-thienyl)-ethoxy-4-butylsulfonate] (PTEBS) and cationic poly(9,9′-bis(6-*N*,*N*,*N*-trimethylammoniumhexyl)fluorene-*alt*-1,4-phenylene)dibromide (PFP-NR3) CPEs with oppositely charged surfactants, Heeley and co-workers proposed a cross-linking aggregation mechanism, whereby multiple polymer chains interact with a single, oppositely charged surfactant molecule.[60] At concentrations approaching the CMC, complexation between the CPE and the surfactant *via* electrostatic and/or hydrophobic interactions leads to locally enhanced concentrations of the surfactant and templated formation of CPE–micelle complexes. The study demonstrated that not only are complementary charges between the CPE and the surfactant required for association, but that length of the surfactant tail must also be sufficiently long to penetrate between the polymer chains.

At surfactant concentrations approaching and above the CMC, the surfactant provides a soft, tunable scaffold with a well-defined structure on which the CPE can be templated, yielding co-assembled nanostructures and supramolecular CPE–surfactant assemblies. The solution phase structure of most common surfactants is well-defined by binary (concentration–temperature) phase diagrams, thus providing a means by which the pattern of this organic template can be designed and exploited to modulate the structural organisation and consequently the optical properties of the co-assembled CPE. Knaapila, Evans and co-workers have recently explored the use of complementary small-angle neutron scattering (SANS) and photoluminescence measurements to probe the internal organisation of the electrostatic CPE–surfactant complexes formed between the cationic polythiophenes poly[3-(6-trimethylammoniumhexyl)thiophene] (P3TMAHT) and poly[3-[6-(*N*-methylimidazolium)hexyl]thiophene] (P3ImiHT) and anionic surfactants (*e.g.* sodium dodecyl sulfate) in D_2O (Fig. 3).[61–63] By exploiting differences in the neutron scattering length densities of the individual components in the CPE–surfactant–D_2O system, SANS enables both the internal and supramolecular organisation of the CPE–surfactant complexes to be probed. Although P3TMAHT and P3ImiHT differ only in the ionic terminal groups on their side chains, subtle differences in the surfactant mole fraction (x) and chemical structure (*e.g.* chain length, head group charge density, perfluorination) result in marked variations in the range and type of complexes formed, ranging from spherical aggregates, to rods and lamellar sheets. These structural transitions are accompanied by concomitant modifications to the optical properties, which include surfactochromic shifts in the solution color from red (P3TMAHT) to violet (x = 1/5 to 1) to yellow (x > 2) and increased vibronic structure in the photoluminescence spectrum, thus providing each complex structure with a unique colorimetric and fluorimetric fingerprint (Fig. 3). The results suggest that P3TMAHT may have potential as an optical sensor platform for the detection of industrially relevant anionic surfactants using dual mode (colorimetric and fluorimetric) detection to selectively identify distinct structural sub-groups.

Self-assembled CPE–surfactant complexes have also been demonstrated as effective interfacial modifiers to improve the performance of bulk-heterojunction (BHJ) solar cells.[64] The active BHJ layer consists of a homogeneous blend of the electron donor and electron acceptor, which are typically poly(3-hexyl thiophene) (P3HT) and [6,6]-phenyl C_{61} butyric acid methyl ester (PCBM), respectively. The addition of a CPE interlayer between the active layer and the metal electrode interface has been shown to significantly enhance device efficiency, which is believed to be due to the formation of dipoles at the organic–metal interface which facilitate electron transport.[65–67] However, the P3HT:PCBM layer is highly hydrophobic and as a result shows limited wettability to the polar CPE layer, resulting in discontinuous film formation.[68] Chang *et al.* have recently shown that the stoichiometric complex formed between P3TMAHT (Fig. 3) and the anionic surfactant sodium dodecyl benzene sulfate (SDBS) could similarly be employed as a cathode interface layer, leading to a 2% increase in the power conversion efficiency relative to the parent device.[64] Complexation with SDBS increased the hydrophobicity of the P3TMAHT interlayer, consequently improving spreading of the film at the organic–metal interface, as inferred from the observed contact angle change from 105° to 70.6° at the P3HT:PCBM film surface. The increased power conversion efficiency was thus attributed to superior film formation and subsequent increased charge transport efficiency at the interface.

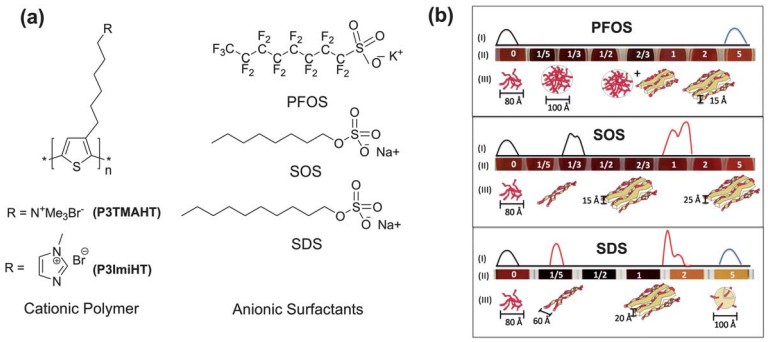

Fig. 3 (a) Structures of cationic polythiophenes and anionic surfactants. (b) Schematic representation of the correlation between the structure and supramolecular organisation of P3TMAHT–(surfactant)$_x$ complexes and the observed optical response. (I) Fluorimetric response represented by changes in emission band shape or wavelength relative to isolated P3TMAHT (black line). Shifts in λ_{em} are indicated by the line color. (II) Observed colorimetric response as function of the surfactant mole fraction, x. (III) Proposed P3TMAHT (red)–surfactant (yellow) complex structures in aqueous solution from SANS. Adapted with permission from ref. 61. Copyright 2012 American Chemical Society.

3.2 CP organogels and surfactogels

In some solvents, conjugated polymers self-assemble into soft supramolecular assemblies or organogels, where physical interactions determine the ordering and packing of the polymer chains over several length scales. Supramolecular organisation can result in a change in the optoelectronic properties. For example, poly(2,5-dialkyl-*p*-phenyleneethylene) (PPE) based gels in toluene exhibit liquid crystallinity at high concentrations[69] and β-phase formation has been observed in poly(fluorene) supramolecular gels in apolar organic solvents.[70] More recently, it has been demonstrated that the PL emission colour of organogels and related spin-coated films of polyfluorene-based poly(tertiary alcohols) (PPFOH) can be modulated by changing the solvent and polymer molecular weight (M_n) (Fig. 4).[71] Above the critical gelation concentration (CGC), hydrogen bonding and π–π stacking interactions promote chain aggregation in non-polar solvents such as toluene, resulting in the formation of organogels. The PL spectrum of the organogel exhibits a broad emission band centred at 465 nm, which becomes increasingly red-shifted as the concentration is increased. Increasing the M_n of the polymer lowers the CGC and simultaneously results in the emergence of a second emission band centred at 560 nm, which is attributed to emission from low energy, hydrogen-bonding assisted, interpolymer complex domains present in the PPFOH gel. The influence of M_n becomes more significant in spin-coated films prepared from PPFOH/toluene solutions: a significant contribution from the low-energy band to the photoluminescence spectrum of the high molecular weight polymer (PPFOH-H) shifts the observed emission colour from blue to pale green/yellow. In polar aprotic solvents such as THF, organogelation is not observed, but the low-energy emission band dominates the photoluminescence spectrum of the corresponding spin-coated films, which appear bright yellow under irradiation (Fig. 4). Thus, by modulating the supramolecular structure of the precursor solution for spin-coating, it is possible to tune the optical properties.

Organogel formation is controlled by factors such as concentration, temperature, solvent and ageing. Hybrid CPE–surfactogels can additionally be formed by complexation with charge compensating surfactants at concentrations above the CGC. For example, Osuji *et al.* showed that in aqueous solution the anionic PTEBS and cationic surfactant cetyl trimethyl ammonium bromide (CTAB) system results in the formation of a optically isotropic hydrogel-like phase at low concentrations (~4 wt%).[72] Concentration of the gel by slow solvent evaporation produces a strongly birefringent sample indicative of a isotropic-liquid crystalline transition at a critical concentration of 35 wt%, resulting in the formation of a hexagonally ordered lyotropic mesophase in which the polymer chains are packed into hexagonally ordered rod-like assemblies. The lyotropic-liquid crystalline tendency of the surfactant is thus imparted on the CPE in the hybrid hydrogel, providing a means by which the optical properties may be modulated. The related P3KHT (poly(3-potassium hexanoate thiophene))–CTAB system also forms a stable supramolecular hydrogel, which upon dilution undergoes a time-dependent coil-to-rod conformational transition, which is manifested by significant changes in the UV/Vis absorption and PL spectra.[73] Following dilution, the system gradually changed colour from orange to brown (after minutes), eventually forming a biphasic deep purple precipitate after weeks. The UV/Vis absorption spectrum is consistent with these changes: the absorbance of the freshly diluted hydrogel occurs at $\lambda_{abs} \sim 430$ nm, with the subsequent evolution of a red-shift centred at 590 nm being observed as a function of time. Similarly the corresponding photoluminescence spectrum exhibits a 50 nm red-shift from $\lambda_{em} \sim 580$ nm to $\lambda_{em} \sim 630$ nm upon ageing. These results are consistent with a time-dependent conformational transition from a coil-like state with twisting and bending between thiophene repeat units (high energy), to a rod-like state that has a smaller dihedral angle between the thiophene rings, effectively extending the conjugation length.

3.3 CPE–polymeric surfactant films

Emissive polymers are often blended with a second inert or active polymer in an attempt to reduce interchain interactions.[8,9] However, the low entropy associated with the mixing of dissimilar polymers typically results in phase separation when blends are cast as thin films from solution. Al-Attar and

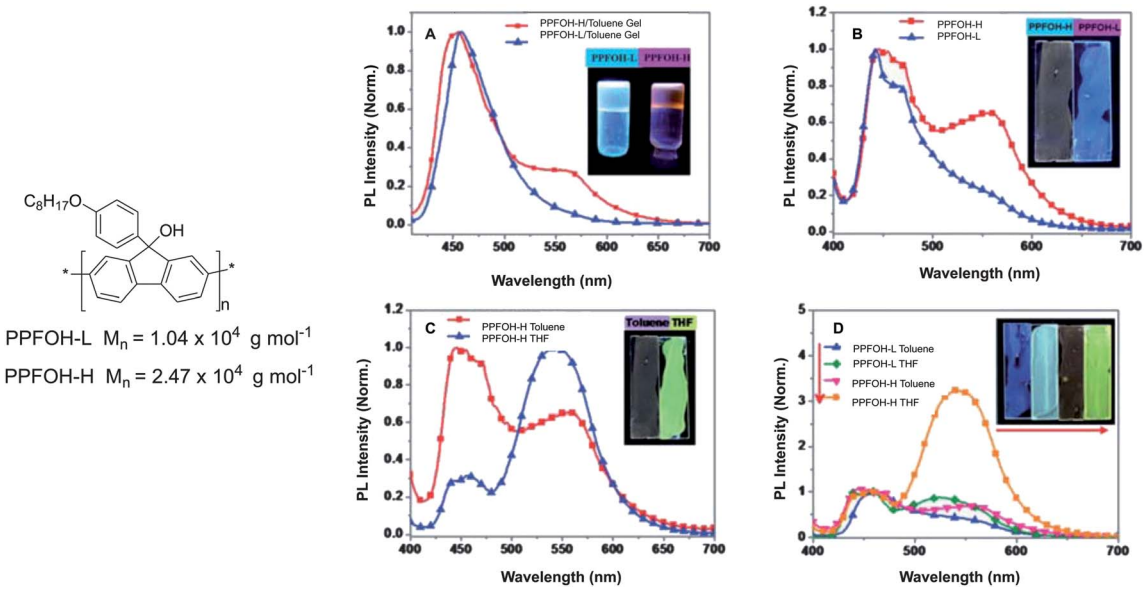

Fig. 4 Structure and optical properties of PPFOH-L and PPFOH-H in various states. (a) PL spectra of PPFOH-L and PPFOH-H/toluene gels. (b) PL spectra of PPFOH-L and PPFOH-H films spin-coated from toluene solutions. (c) PL spectra of PPFOH-H films spin-coated from toluene and THF solutions. (d) PL spectra of PPFOH-H and PPFOHL films spin-coated from toluene and THF solutions (concentration: 2 mg mL^{-1}). Adapted from ref. 71.

Monkman have recently shown that this problem may be overcome using mixtures of water-soluble CPEs, *e.g.* PFP-NR3, with polymeric surfactants such as poly(vinyl alcohol) (PVA) to form stable films of the blend that are homogeneously mixed at the nanoscale.[74] The PVA functions both as a surfactant that effectively breaks up CPE aggregates and also as a cage which efficiently locks the isolated chains in place *via* hydrogen bonding interactions between neighbouring PVA chains and residual water of crystallisation. Opening and closing of the PVA cage can be controlled by temperature. At 80–90 °C in solution, hydrogen bonding interactions between neighbouring chains are disrupted, PVA is completely soluble and the cage is open. Spin coating or drop casting of the hot CPE/PVA solution, followed by fast drying, results in rapid crystallisation of the PVA network, and closing of the cage. Complete isolation of the CPE chains within the hydrogen-bonded PVA superstructure leads to an increase in the PL lifetime and a concomitant increase in the PL quantum yield, from $\Phi_{PL} = 0.08$ in the pure PFP-NR3 film, to $\Phi_{PL} = 0.55$ in the PFP-NR3/PVA blend. Even more remarkable, then, is the observance of room-temperature phosphorescence from the PFP-NR3/PVA drop cast film, indicating the PVA hydrogen bonded network efficiently confines relaxation of the CPE backbone to isolated chains, with very little or no exciton diffusion. One limitation of electroluminescence in organic materials is that charge injection produces both singlet and triplet excited states, in the statistical ratio 1 : 3. Since only the singlet state is normally luminescent, this normally reduces the maximum efficiency possible from these devices to 25%. Since these PFP-NR3/PVA blends are able to harvest both singlet and triplet excitons, they may show considerable promise as the emissive layer in polymer light-emitting diodes with the potential of approaching the theoretical 100% photoluminescence efficiency.[74]

4 Organic–inorganic hybrid CP materials

Organic–inorganic hybrids combine the advantages of "soft" organic and "hard" inorganic building blocks in a single material. The properties of the hybrid are governed by the individual contributions of both the organic and inorganic components, as well as the inner interfacial contributions.[75] Hybrids incorporating small organic lumophores have been extensively examined for the development of robust, light-emitting platforms[76] and attention has now turned towards the preparation of conjugated polymer based analogues. The incorporation of CPs into an inorganic matrix introduces multiple possibilities. It enhances the potential for technology-transfer from the laboratory to the consumer, *e.g.* for solid-state sensors and displays, whilst simultaneously providing an alternative route to exert control over polymer conformation and orientation,[11,77,78] as well as improving environmental stability.[78,79] Moreover, weak physical interactions can also be exploited and coordinated to yield desirable morphologies at the organic–inorganic interface.[79]

The preparation of CP–organic–inorganic hybrids is non-trivial. Sol–gel chemistry is typically the preferred route to composite materials, however achieving miscibility between the hydrophilic inorganic oxide sol–gel precursors, the hydrophobic conjugated polymer and the aqueous processing media is challenging. Moreover, in the absence of specific interactions between the two components, aggregation of the organic constituent in the inorganic matrix often occurs during the sol–gel process, leading to macroscale phase separation. A number of methods have been proposed to address these difficulties, which include (i) the use of water-soluble CPEs;[79] (ii) introducing a zwitterionic mediator;[80] (iii) the use of polar aprotic

solvents;[78,81,82] and (iv) co-templating with non-ionic surfactants.[77,78,81–83] We will now consider each approach in turn.

The use of conjugated polyelectrolytes as the organic component both improves solubility in the sol–gel media and facilitates homogeneous mixing of the organic–inorganic components *via* electrostatic interactions. Homogeneous polyacetylene–silica[84,85] and polythiophene–silica[86] and –titania[87] hybrids have been successfully prepared using the sol–gel method by exploiting ionic interactions between cationic groups on the CPE side chain and anionic silanol moieties. Evans and co-workers have shown that the charge on the CPE chains can critically affect the extent of phase aggregation at the organic–inorganic interface in poly(fluorene)–silica hybrids.[79] Silica nanocomposites prepared from the anionic poly[9,9-bis(4-sulfonylbutoxyphenyl)fluorene-2,7-diyl-*alt*-1,4-phenylene] (PBS-PFP) and cationic PFP-NR3 are homogeneously mixed at the micron scale, but simultaneously exhibit nanoscale separation at the phase interface. Solid-state ^{29}Si magic-angle spinning (MAS) NMR, AFM and PL measurements indicated that immiscibility at the nanoscale is more pronounced for the cationic PFP-NR3, which is attributed to a more homogenous uptake of the anionic PBS-PFP into the condensing silica network, mediated by hydrogen bonding interactions between terminal SO_3^- units on the CPE and silanol groups. In contrast, the cationic NMe_3^+ groups are able to interact with the inorganic component only *via* much weaker van der Waals forces. Charge-mediated aggregation may thus provide the key to controlling nanophase separation, whilst enabling continuity of the individual phases at longer length scales. This could have important implications for the design of CP–organic–inorganic hybrid materials for photovoltaics, which whilst requiring that each phase maintains continuity through the active layer to provide a continuous pathway for carrier transport to the electrodes, simultaneously demands the presence of high surface area, interpenetrating networks of the electron donor and acceptor to minimise the charge carrier diffusion distance. The poly(fluorene)–silica hybrids retain the intense blue photoluminescence of the parent CPE, which is efficiently quenched by nitroaromatic vapors, suggesting that these materials may also show potential as prototype platforms for explosives detection. Notably, after quenching, the PL is easily regenerated over multiple quenching cycles, indicating that these materials may find application as robust solid-state sensors.

Neutral poly(fluorenes) and poly(phenylene ethylene)s have also been incorporated into silica composites prepared under non-aqueous sol–gel conditions (*e.g.* in $CHCl_3$, formic acid) in the presence of room-temperature ionic liquids (RTILs).[80,88] Such hybrids are termed *ionogels*, since the ionic liquid is confined within the solid oxide host network whilst simultaneously retaining its liquid nature. The inherent amphiphilicity of RTILs promotes physical interactions at the RTIL–silica interface (*e.g.* hydrogen bonding, π–π stacking) which can be exploited to template organised structures into mesoporous silica.[89] We recently demonstrated that cooperative interactions at the phase interface could similarly be used to promote localisation of the three components in poly(9,9-dioctylfluorene)-silica-$[Bmim]^+[Tf_2N]^-$ (1-butyl-3-methyl-imidazolium bis(trifluoromethanesulfonyl)imide) ionogels within either hydrophilic or hydrophobic domains (Fig. 5).[80] PFO was observed to preferentially occupy the hydrophobic environment created by π–π stacking interactions between $[Bmim]^+$ cations, driving the formation of planar, stacked PFO aggregates. Concomitantly, hydrogen bonding with free silanol groups promotes directed orientation of the $[Tf_2N]^-$ anion along the silica walls. Upon incorporation into the ionogel, the UV/Vis absorption and PL spectra are both significantly red-shifted compared to PFO in solution, indicating the polymer adopts a more rigid, planar conformation with extended π conjugation in the solid state. This behavior is consistent with a transition from the disordered α-phase to the formation of the β-phase in the ionogel, in which individual PFO chains adopt a π–π stacked structure.

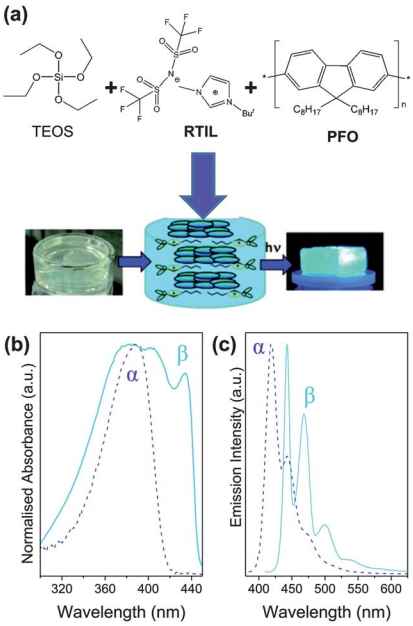

Fig. 5 (a) Schematic representation of the proposed stacking mechanism that promotes β-phase formation in PFO-ionogels. (b) UV/Vis absorption and (c) PL spectra for PFO in $CHCl_3$ (blue dashed line) and PFO-ionogel (cyan solid line) demonstrate β-phase formation. Adapted from ref. 80.

Co-assembly approaches can also be used to introduce CPs into mesostructured inorganic oxide films of titania or silica. Non-ionic amphiphilic surfactants such as Brij™ and Pluronics™ are well-known to act as structure directing agents (SDAs) for the formation of templated, ordered mesoporous inorganic materials using sol–gel conditions.[90,91] Mesostructured films are prepared by dip-coating a mixture of the inorganic oxide precursor and the surfactant onto a substrate; subsequent evaporation-induced concentration gradients promote the formation of highly ordered, self-assembled inorganic oxide–surfactant mesostructures, which are frozen in place upon polymerisation of the inorganic phase. The addition of a conjugated polymer into the precursor solution promotes co-assembly of the hydrophobic CP, the amphiphilic SDA and the hydrophilic inorganic oxide, circumventing macrophase separation.[77,78,81–83] By modifying parameters such as the

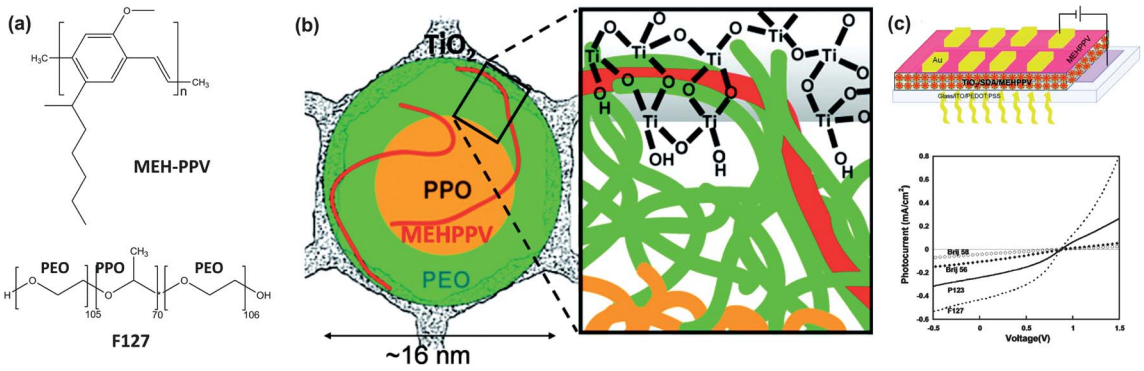

Fig. 6 (a) Structure of MEH-PPV and the structure-directing agent F127. (b) Schemation representation of the interfacial organisation of a single mesochannel in MEH-PPV–F127–titania films (from NMR and TEM results). (c) Photovoltaic device structure and corresponding current–voltage curves. Adapted with permission from ref. 92. Copyright 2011 American Chemical Society.

surfactant type, concentration, solvent and temperature, it is possible to fabricate films exhibiting a variety of morphologies, including hexagonal closed-packed, cubic and lamellar structural motifs. Frey and coworkers have shown that the chemical composition and structural organisation at the organic–inorganic interface can have a significant influence on the photovoltaic properties of these materials.[77,92] In a comprehensive study they used a series of ethylene oxide (EO)-propylene oxide (PO) block-co-polymer surfactants as structure-directing agents to template the formation of MEH-PPV–titania cubic mesostructured films.[92] The length of the hydrophilic EO segments and the type of hydrophobic segment were shown to critically influence the extent of interfacial interaction, such that SDAs containing long hydrophilic segments and moderately hydrophobic PO blocks (*e.g.* F127) promoted enhanced mixing at the CP–titania interface (Fig. 6). Improved interfacial contact resulted in increased PL decay rates and high photocurrent generation in these films compared to analogous MEH-PPV–titania films templated using P123 or Brij58, which contain a more extensive hydrophobic component. Enhanced contact between the CP and the titania framework thus results in efficient electron transfer at the phase interface, yielding correspondingly higher photovoltaic efficiencies for the MEH-PPV–F127–titania films (0.082% conversion efficiency *vs.* 0.006% for MEH-PPV–Brij58–titania) (Fig. 6). Controlled interfacial engineering may therefore provide a route to improved efficiency in hybrid photovoltaic devices.

5 Summary and outlook

Molecular design and strategic chemical synthesis enable facile tuning of the optoelectronic properties of individual conjugated polymer chains through judicious selection of the repeat unit. However, in real-life applications conjugated polymers do not exist as discrete, non-interacting chains, but instead as macroscopic assemblies in a variety of states including films, fibres and interfaces. The packing of the individual polymer chains in these different states will determine the electronic coupling, and consequently the optoelectronic properties. If organic electronic devices are to achieve higher performance levels, then understanding the factors which drive intermolecular organisation and the development of chemical design strategies that provide control over it must be key priorities. As the examples presented in this Highlight illustrate, self-assembly may indeed provide the solution to this challenge, offering a mechanism by which individual components may be assembled into larger, more-ordered functional ensembles. However, the challenge of understanding the interplay between the different weak physical interactions which drive intermolecular organisation in these materials remains unsolved. Success in this approach will therefore require that chemical synthesis and self-assembly are developed in tandem. Advances in synthetic design mean that conjugated polymers are no longer restricted to the propagation of a single repeat unit and as demonstrated above, a variety of structural arrangements, such as block copolymer, dendrimers and star-burst polymers, are now readily accessible.[26] Similarly, structural modifications of individual fragments of the polymer chain may provide a mechanism by which the self-assembly of multiple chains can be directed. This may be at a fundamental level, for example the strategic introduction of functional groups that promote weak physical interactions such as hydrogen bonding or van der Waals forces. Alternatively, it may involve a more sophisticated demonstration of the exploitation of size, geometry and orientation of the repeat unit to direct intermolecular assembly. The role of side chains in controlling both solubility and self-assembly has already been established. However, many structural variations in terms of the topology, chemical composition and distribution of side chains across the backbone structure have yet to be explored. The molecular weight and polydispersity of the polymer chains are also key considerations, since these will also influence the supramolecular organisation and morphology. The parallel evolution of judicious molecular design and chemical synthesis should provide a pathway to targeted self-assembly in both single component and hybrid materials, enabling the preparation of unprecedented structures and patterns at the nanoscale with the added benefit of incorporated functionality. This capability will open up an exciting avenue for the transfer of self-assembled conjugated polymer materials from the laboratory to the market place and

take us closer to the ultimate goal of deciphering the complex relationship between molecular structure, supramolecular organisation and device performance.

References

1 D. Gendron and M. Leclerc, *Energy Environ. Sci.*, 2011, **4**, 1225–1237.
2 G. Li, R. Zhu and Y. Yang, *Nat. Photonics*, 2012, **6**, 153–161.
3 A. Facchetti, *Chem. Mater.*, 2010, **23**, 733–758.
4 H. N. Tsao, D. M. Cho, I. Park, M. R. Hansen, A. Mavrinskiy, D. Y. Yoon, R. Graf, W. Pisula, H. W. Spiess and K. Müllen, *J. Am. Chem. Soc.*, 2011, **133**, 2605–2612.
5 T. Q. Nguyen, R. C. Kwong, M. E. Thompson and B. J. Schwartz, *Appl. Phys. Lett.*, 2000, **76**, 2454.
6 J. Liu, Y. Shi and Y. Yang, *Adv. Funct. Mater.*, 2001, **11**, 420–424.
7 R. R. Sondergaard, M. Hosel and F. C. Krebs, *J. Polym. Sci., Part B: Polym. Phys.*, 2013, **51**, 16–34.
8 J. Chappell, D. G. Lidzey, P. C. Jukes, A. M. Higgins, R. L. Thompson, S. O'Connor, I. Grizzi, R. Fletcher, J. O'Brien, M. Geoghegan and R. A. L. Jones, *Nat. Mater.*, 2003, **2**, 616–621.
9 M. Knaapila, H. L. Vaughan, T. P. A. Hase, R. C. Evans, R. Stepanyan, M. Torkkeli, H. D. Burrows, U. Scherf and A. P. Monkman, *Macromolecules*, 2010, **43**, 299–305.
10 J. Y. Park and R. C. Advincula, *Soft Matter*, 2011, **7**, 9829–9843.
11 T.-Q. Nguyen, J. Wu, V. Doan, B. J. Schwartz and S. H. Tolbert, *Science*, 2000, **288**, 652–656.
12 K.-H. Lo, R.-M. Ho, Y.-M. Liao, C.-S. Hsu, F. Massuyeaum, Y.-C. Zhao, S. Lefrant and J.-L. Duvail, *Adv. Funct. Mater.*, 2011, **21**, 2729–2736.
13 F. Cucinotta, F. Carniato, G. Paul, S. Bracco, C. Bisio, S. Caldarelli and L. Marchese, *Chem. Mater.*, 2011, **23**, 2803–2809.
14 E. Tekin, D. A. M. Egbe, J. M. Kranenburg, C. Ulbricht, S. Rathgeber, E. Birckner, N. Rehmann, K. Meerholz and U. S. Schubert, *Chem. Mater.*, 2008, **20**, 2727–2735.
15 K. Lee, H.-J. Kim and J. Kim, *Adv. Funct. Mater.*, 2012, **22**, 1076–1086.
16 L. Zhou, J. L. Geng, G. Wang, J. Liu and B. Liu, *Polym. Chem.*, 2013, DOI: 10.1039/C3PY21080D.
17 M. Aryal, K. Trivedi and W. C. Hu, *ACS Nano*, 2009, **3**, 3085–3090.
18 J. Vogelsang, T. Adachi, J. Brazard, D. A. V. Bout and P. F. Barbara, *Nat. Mater.*, 2011, **10**, 942–946.
19 G. A. Ozin, K. Hou, B. V. Lotsch, L. Cademartiri, D. P. Puzzo, F. Scotognella, A. Ghadimi and J. Thomson, *Mater. Today*, 2009, **12**, 12–23.
20 K. V. Rao, K. K. R. Datta, M. Eswaramoorthy and S. J. George, *Chem.–Eur. J.*, 2012, **18**, 2184–2194.
21 L. R. Xu, L. Yang and S. B. Lei, *Nanoscale*, 2012, **4**, 4399–4415.
22 K. Rahimi, I. Botiz, N. Stingelin, N. Kayunkid, M. Sommer, F. P. V. Koch, H. Nguyen, O. Coulembier, P. Dubois, M. Brinkmann and G. Reiter, *Angew. Chem., Int. Ed.*, 2012, **51**, 11131.
23 Y. Liang, H. Wang, S. Yuan, Y. Lee, L. Gan and L. Yu, *J. Mater. Chem.*, 2007, **17**, 2183–2194.
24 L. Xu, L. Yang and S. Lei, *Nanoscale*, 2012, **4**, 4399–4415.
25 G. M. Whitesides and B. Grzybowski, *Science*, 2002, **295**, 2418–2421.
26 Z. B. Henson, K. Mullen and G. C. Bazan, *Nat. Chem.*, 2012, **4**, 699–704.
27 M. Ballauff, *Angew. Chem., Int. Ed. Engl.*, 1989, **28**, 253–267.
28 H. Jiang, P. Taranekar, J. R. Reynolds and K. S. Schanze, *Angew. Chem., Int. Ed. Engl.*, 2009, **48**, 4300–4316.
29 A. Duarte, K.-Y. Pu, B. Liu and G. C. Bazan, *Chem. Mater.*, 2011, **23**, 501–515.
30 S. Wang and G. C. Bazan, *Chem. Commun.*, 2004, 2508–2509.
31 H. D. Burrows, S. M. Fonseca, C. L. Silva, A. A. C. C. Pais, M. J. Tapia, S. Pradhan and U. Scherf, *Phys. Chem. Chem. Phys.*, 2008, **10**, 4420–4428.
32 A. T. Marques, H. D. Burrows, J. S. S. d. Melo, A. J. M. Valente, L. L. G. Justino, U. Scherf, E. Fron, S. Rocha, J. Hofkens, E. W. Snedden and A. P. Monkman, *J. Phys. Chem. B*, 2012, **116**, 7548–7559.
33 T. M. Swager, C. J. Gil and M. S. Wrighton, *J. Phys. Chem.*, 1995, **99**, 4886–4893.
34 C. Tan, E. Atas, J. G. Muller, M. R. Pinto, V. D. Kleiman and K. S. Schanze, *J. Am. Chem. Soc.*, 2004, **126**, 13685–13694.
35 Y. Hong, J. W. Y. Lam and B. Z. Tang, *Chem. Soc. Rev.*, 2011, **40**, 5361–5388.
36 Y. Hong, J. W. Y. Lam and B. Z. Tang, *Chem. Commun.*, 2009, 4332–4353.
37 J. Liu, J. W. Y. Lam and B. Z. Tang, *Chem. Rev.*, 2009, **109**, 5799–5867.
38 A. Qin, C. K. W. Jim, Y. Tang, J. W. Y. Lam, J. Liu, F. Mahtab, P. Gao and B. Z. Tang, *J. Phys. Chem. B*, 2008, **112**, 9281–9288.
39 C. Wu, B. Bull, C. Szymanski, K. Christensen and J. McNeill, *ACS Nano*, 2008, **2**, 2415–2423.
40 J. Pecher and S. Mecking, *Chem. Rev.*, 2010, **110**, 6260–6279.
41 D. Tuncel and H. V. Demir, *Nanoscale*, 2010, **2**, 484–494.
42 A. Kaeser, I. Fischer, R. Abbel, P. Besenius, D. Dasgupta, M. A. J. Gillisen, G. Portale, A. L. Stevens, L. M. Herz and A. P. H. J. Schenning, *ACS Nano*, 2013, **7**, 408–416.
43 A. L. Stevens, A. Kaeser, A. P. H. J. Schenning and L. M. Herz, *ACS Nano*, 2012, **6**, 4777–4787.
44 B. Xu, M. Lu, J. Kang, D. Wang, J. Brown and Z. Peng, *Chem. Mater.*, 2005, **17**, 2841–2851.
45 P. C. Yin, L. Jin, D. Li, P. Cheng, D. V. Vezenov, E. Bitterlich, X. Wu, Z. H. Peng and T. B. Liu, *Chem.–Eur. J.*, 2012, **18**, 6754–6758.
46 T. Liu, E. Diemann, H. Li, A. W. M. Dress and A. Müller, *Nature*, 2003, **426**, 59–60.
47 T. Liu, *Langmuir*, 2010, **26**, 9202–9213.
48 W. Qi and L. L. Wu, *Polym. Int.*, 2009, **58**, 1217–1225.
49 U. Scherf, A. Gutacker and N. Koenen, *Acc. Chem. Res.*, 2008, **41**, 1086–1097.
50 U. Scherf, S. Adamczyk, A. Gutacker and N. Koenen, *Macromol. Rapid Commun.*, 2009, **30**, 1059–1065.
51 L. Ying, P. Zalar, S. D. Collins, Z. Chen, A. A. Mikhailovsky, T.-Q. Nguyen and G. C. Bazan, *Adv. Mater.*, 2012, **24**, 6496–6501.

52 A. Gutacker, S. Adamczyk, A. Helfer, L. E. Garner, R. C. Evans, S. M. Fonseca, M. Knaapila, G. C. Bazan, H. D. Burrows and U. Scherf, *J. Mater. Chem.*, 2010, **20**, 1423–1430.
53 G. Tu, H. Li, M. Forster, R. Heiderhoff, L. J. Balk, R. Sigel and U. Scherf, *Small*, 2007, **3**, 1001–1006.
54 M. Knaapila, R. C. Evans, A. Gutacker, V. M. Garamus, M. Torkkeli, S. Adamczyk, M. Forster, U. Scherf and H. D. Burrows, *Langmuir*, 2010, **26**, 5056–5066.
55 A. Gutacker, N. Koenen, U. Scherf, S. Adamczyk, J. Pina, S. M. Fonseca, A. J. M. Valente, R. C. Evans, J. S. de Melo, H. D. Burrows and M. Knaapila, *Polymer*, 2010, **51**, 1898–1903.
56 H. D. Burrows, V. M. M. Lobo, J. Pina, M. L. Ramos, J. Seixas de Melo, A. J. M. Valente, M. J. Tapia, S. Pradhan and U. Scherf, *Macromolecules*, 2004, **20**, 7425–7427.
57 J. J. Lavigne, D. L. Broughton, J. N. Wilson, B. Erdogan and U. H. F. Bunz, *Macromolecules*, 2004, **36**, 7409–7412.
58 L. Chen, S. Xu, D. McBranch and D. Whitten, *J. Am. Chem. Soc.*, 2000, **122**, 9302–9303.
59 I. Echavarri Franco, P. Lorchat, J.-P. Lamps, M. Schmutz, A. Schröder, J.-M. Catala, J. Combet and F. Schosseler, *Langmuir*, 2012, **28**, 4815–4828.
60 M. E. H. Heeley, J. K. Gallaher, T. L. Nguyen, H. Y. Woo and J. M. Hodgkiss, *Chem. Commun.*, 2013, **49**, 4235–4237.
61 R. C. Evans, M. Knaapila, N. Willis-Fox, M. Kraft, A. Terry, H. D. Burrows and U. Scherf, *Langmuir*, 2012, **28**, 12348–12356.
62 M. Knaapila, R. C. Evans, V. M. Garamus, L. Almásy, N. K. Székely, A. Gutacker, U. Scherf and H. D. Burrows, *Langmuir*, 2010, **26**, 15634–15643.
63 M. Knaapila, R. C. Evans, A. Gutacker, V. M. Garamus, N. K. Székely, U. Scherf and H. D. Burrows, *Soft Matter*, 2011, **7**, 6863–6872.
64 Y. M. Chang, R. Zhu, E. Richard, C. C. Chen, G. Li and Y. Yang, *Adv. Funct. Mater.*, 2012, **22**, 3284–3289.
65 J. H. Seo, A. Gutacker, Y. Sun, H. Wu, F. Huang, Y. Cao, U. Scherf, A. J. Heeger and G. C. Bazan, *J. Am. Chem. Soc.*, 2011, **133**, 8416–8419.
66 H. Choi, J. S. Park, E. Jeong, G.-H. Kim, B. R. Lee, S. O. Kim, M. H. Song, H. Y. Woo and J. Y. Kim, *Adv. Mater.*, 2011, **23**, 2759–2763.
67 Z. He, C. Zhang, X. Xu, L. Zhang, L. Huang, J. Chen, H. Wu and Y. Cao, *Adv. Mater.*, 2011, **23**, 3086–3089.
68 K. Yao, L. Chen, Y. W. Chen, F. Li and P. S. Wang, *J. Mater. Chem.*, 2011, **21**, 13780–13784.
69 W. Y. Huang, S. Matsuoka, T. K. Kwei and Y. Okamoto, *Macromolecules*, 2001, **34**, 7166–7171.
70 Z.-Q. Lin, N.-E. Shi, Y.-B. Li, D. Qiu, L. Zhang, J.-Y. Lin, J.-F. Zhao, C. Wang, L.-H. Xie and W. Huang, *J. Phys. Chem. C*, 2011, **115**, 4418–4424.
71 J. Lin, A. Yu, W. Zhu, G. Xing, Z. Lin, S. Yang, L. Xie, C. Niu and W. Huang, *Polym. Chem.*, 2013, **4**, 477–483.
72 S. Zhang, L. D. Pfefferle and C. O. Osuji, *Macromolecules*, 2010, **43**, 7549–7555.
73 C. D. Danesh, N. S. Starkweather and S. Zhang, *J. Phys. Chem. B*, 2012, **116**, 12887–12894.
74 H. A. Al-Attar and A. P. Monkman, *Adv. Funct. Mater.*, 2012, **22**, 3824–3832.
75 C. Sanchez, P. Belleville, M. Popall and L. Nicole, *Chem. Soc. Rev.*, 2011, **40**, 696–753.
76 X. H. Yang, T. Giovenzana, B. Feild, G. E. Jabbour and A. Sellinger, *J. Mater. Chem.*, 2012, **22**, 12689–12694.
77 S. Neyshtadt, M. Kalina and G. L. Frey, *Adv. Mater.*, 2008, **20**, 2541–2546.
78 S. Kirmayer, E. Dovgolevsky, M. Kalina, E. Lakin, J. D. Caders, A. Epping, A. Fernández-Arteaga, C. Rodríguez-Abreu, B. F. Chmelka and G. L. Frey, *Chem. Mater.*, 2008, **20**, 3745–3756.
79 R. C. Evans, A. G. Macedo, S. Pradhan, U. Scherf, L. D. Carlos and H. D. Burrows, *Adv. Mater.*, 2010, **22**, 3032–3037.
80 R. C. Evans and P. C. Marr, *Chem. Commun.*, 2012, **48**, 3742–3744.
81 E. Dovgolevsky, S. Kirmayer, E. Lakin, Y. Yang, C. J. Brinker and G. L. Frey, *J. Mater. Chem.*, 2008, **18**, 423–436.
82 A. Keller, S. Kirmayer, T. Segal-Peretz and G. L. Frey, *Langmuir*, 2012, **28**, 1506–1514.
83 T. Segal-Peretz, O. Leman, A. M. Nardes and G. L. Frey, *J. Phys. Chem. C*, 2012, **116**, 2024–2032.
84 T. Ogoshi and Y. Chujo, *Macromolecules*, 2005, **38**, 9110–9116.
85 M. Kubo, C. Takimoto, Y. Minami, T. Uno, T. Itoh and M. Shoyama, *Macromolecules*, 2005, **38**, 7314–7320.
86 S. Clément, A. Tizit, S. Desbief, A. Mehdi, J. De Winter, P. Gerbaux, R. Lazzaroni and B. Boury, *J. Mater. Chem.*, 2011, **21**, 2733–2739.
87 F. Boon, A. Thomas, G. Clavel, D. Moerman, J. De Winter, D. Laurencin, O. Coulembier, P. Dubois, P. Gerbaux, R. Lazzaroni, S. Richeter, A. Mehdi and S. Clement, *Synth. Met.*, 2012, **162**, 1615–1622.
88 N. Cheminet, T. Jarrosson, J.-P. Lere-Porte, F. Serein-Spirau, L. Cury, J. Moreau, L. Viau and A. Vioux, *J. Mater. Chem.*, 2011, **21**, 13588–13593.
89 Y. Zhou, J. H. Schattka and M. Antonietti, *Nano Lett.*, 2004, **4**, 477–481.
90 D. Y. Zhao, J. L. Feng, Q. S. Huo, N. Melosh, G. H. Fredrickson, B. F. Chmelka and G. D. Stucky, *Science*, 1998, **279**, 548–552.
91 S. A. Bagshaw, E. Prouzet and T. J. Pinnavaia, *Science*, 1995, **269**, 1242–1244.
92 S. Neyshtadt, J. P. Jahnke, R. J. Messinger, A. Rawal, T. S. Peretz, D. Huppert, B. F. Chmelka and G. L. Frey, *J. Am. Chem. Soc.*, 2011, **133**, 10119–10133.

